frontiers in Microbiology

ORIGINAL RESEARCH
published: 10 July 2020
doi: 10.3389/fmicb.2020.01603

HIV-2-Infected Macrophages Produce and Accumulate Poorly Infectious Viral Particles

Ester Gea-Mallorquí[1†], Laurent Zablocki-Thomas[1], Mathieu Maurin[1], Mabel Jouve[2], Vasco Rodrigues[1], Nicolas Ruffin[1] and Philippe Benaroch[1*]*

[1] Institut Curie, PSL* Research University, INSERM U932, Paris, France, [2] Institut Curie, PSL* Research University, UMR3216, Paris, France

OPEN ACCESS

Edited by:
Guido Poli, Vita-Salute San Raffaele University, Italy

Reviewed by:
Eric O. Freed, National Cancer Institute at Frederick, United States
Jérôme Bouchet, Paris Descartes University, France
Christel Vérollet, UMR 5089 Institut de Pharmacologie et de Biologie Structurale (IPBS), France

***Correspondence:**
Nicolas Ruffin
nicolas.ruffin@ki.se
Philippe Benaroch
philippe.benaroch@curie.fr

†Present address:
Ester Gea-Mallorquí, Nuffield Department of Medicine, University of Oxford, Oxford, United Kingdom

Specialty section:
This article was submitted to Virology, a section of the journal Frontiers in Microbiology

Received: *25 March 2020*
Accepted: *18 June 2020*
Published: *10 July 2020*

Citation:
Gea-Mallorquí E, Zablocki-Thomas L, Maurin M, Jouve M, Rodrigues V, Ruffin N and Benaroch P (2020) HIV-2-Infected Macrophages Produce and Accumulate Poorly Infectious Viral Particles. Front. Microbiol. 11:1603. doi: 10.3389/fmicb.2020.01603

A significant proportion of HIV-2-infected patients exhibit natural virological control that is generally absent from HIV-1-infected patients. Along with $CD4^+$ T cells, HIV-1 targets macrophages which may contribute to viral spreading and the latent reservoir. We have studied the relationship between macrophages and HIV-2, focusing on post-entry steps. HIV-2-infected monocyte-derived macrophages (MDMs) produced substantial amounts of viral particles that were largely harbored intracellularly. New viruses assembled at the limiting membrane of internal compartments similar to virus-containing compartments (VCCs) described for HIV-1. VCCs from MDMs infected with either virus shared protein composition and morphology. Strikingly, HIV-2 Gag was mostly absent from the cytosol and almost exclusively localized to the VCCs, whereas HIV-1 Gag was distributed in both locations. Ultrastructural analyses of HIV-2-infected MDMs revealed the presence of numerous VCCs containing both immature and mature particles in the lumen. HIV-2 particles produced *de novo* by MDMs were poorly infectious in reporter cells and in transmission to activated T cells through a process that appeared independent of BST2 restriction. Rather than being involved in viral spreading, HIV-2-infected macrophages may represent a cell-associated source of viral antigens that can participate in the immune control of HIV-2 infection.

Keywords: macrophages, HIV-2, viral assembly, virus-containing compartment, restriction factors, HIV transmission to T cells, viral reservoir

INTRODUCTION

Macrophages are key players of the innate immune system and can rapidly respond to many pathogens. In HIV-1 infection, macrophages are also targets in which the virus replicates and accumulates. Infected macrophages tend to resist the cytopathic effects of HIV-1, can survive for long periods of time (Igarashi et al., 2001; Swingler et al., 2007) and have been found in many tissues from infected individuals (Cribbs et al., 2015). The role of macrophages in the physiopathology of

Abbreviations: AIDS, Acquired Immune Deficiency Syndrome; AZT, azidothymidine; BST2, bone marrow stromal cell antigen 2; CA, capsid; cART, combined anti-retroviral therapy; DCs, dendritic cells; eATP, extracellular ATP; gRNA, genomic RNA; HIV-2, human immunodeficiency virus 2; MA, matrix; MDDC, Monocyte-derived dendritic cells; MDMs, monocyte-derived macrophages; MFI, mean fluorescence intensity; MOI, multiplicity of infection; PBMC, peripheral blood mononuclear cells; RT, reverse transcription; SAMHD1, SAM and HD domain containing deoxynucleoside triphosphate triphosphohydrolase 1; VCCs, virus-containing compartments; VSV-G, vesicular stomatitis virus G; WT, wild type.

the HIV infection has long been debated (Wacleche et al., 2018; Kruize and Kootstra, 2019), but they are known to be involved in the brain, with the development of HIV-1-associated neurological disorders (Koppensteiner et al., 2012).

The importance of macrophages in the formation of a viral reservoir in infected patients has received support from several studies performed in macaques and humanized mice (Honeycutt et al., 2016, 2017; Araínga et al., 2017). HIV-1 infected tissue macrophages have been recently found in the liver and urethra in samples from individuals undergoing cART (Kandathil et al., 2018; Ganor et al., 2019). The persistent inflammation observed in HIV-1-infected patients also appears to involve macrophages (Clayton et al., 2017). A large body of work has characterized the HIV-1 life-cycle in macrophages (see Rodrigues et al., 2017), the impact of the infection on macrophage function (Mazzolini et al., 2010; Verollet et al., 2014), and the sensing mechanisms involved (Chattergoon et al., 2014; Decalf et al., 2017; Nasr et al., 2017). In contrast to HIV-1, very few studies have evaluated the role of macrophages in HIV-2 infection.

HIV-2 is the second causative agent for AIDS and leads to an immunodeficiency syndrome that is essentially identical to that of HIV-1 once $CD4^+$ T cell counts drop. Both viruses share comparable genetic organization, structural architecture, and most virological features. Despite this close relationship, the clinical progression of HIV-2 to AIDS is much slower compared to HIV-1 and may reflect better immune control of the infection (Marlink et al., 1994; Nyamweya et al., 2013; Esbjörnsson et al., 2019). A much larger proportion of people with HIV-2 infection exhibit long-term viral control without ART than is seen in HIV-1 infection (van der Loeff et al., 2010).

It is not yet understood how the better control of HIV-2 infection is induced and maintained. Specific features of the HIV-2 replication cycle may contribute to the differences observed in the pathophysiology. The proviral loads (the number of copies of HIV DNA integrated into circulating $CD4^+$ T cells) in infected patients are similar for the two viruses (Rowland-Jones and Whittle, 2007). In contrast to HIV-1, the number of free circulating viral particles estimated as the circulating viral load in plasma is substantially lower and usually undetectable in HIV-2-infected individuals (Popper et al., 2000; Damond et al., 2002).

Lower levels of circulating virus have been associated with a decreased rate of vertical and horizontal transmission in HIV-2 compared to HIV-1 (Nyamweya et al., 2013). Although, it is estimated that 30–40% of HIV-2 infected people have low or undetectable viral loads (van der Loeff et al., 2010), ongoing viral replication still occurs in HIV-2-infected patients (Soares et al., 2011; Fernandes et al., 2014). However, a recent longitudinal study indicates that without ART treatment, HIV-2-infected individuals have still a high probability of developing and dying from AIDS despite the longer time to progress (Esbjörnsson et al., 2019).

How the specific host immune response contributes to the low viral loads observed in HIV-2 infection remains unclear. Studying a cohort of HIV-2 long-term non-progressors from Gambia, viral control clearly correlated with the presence of a gag-specific $CD8^+$ T-cell response (Leligdowicz et al., 2007). In another cohort a strong polyfunctional $CD8^+$ T cell response specific for Gag was associated with HIV-2 viral control (de Silva et al., 2013). However, the Gag-specific $CD8^+$ T cell responses were absent in 58% of HIV-2 viraemic individuals and the Gag-specific $CD8^+$T cells exhibited features of low effector cytotoxic capacity (de Silva et al., 2013). The presence of broad and potent neutralizing antibodies in HIV-2-infected individuals at either extreme of the viral load/clinical spectrum does not correlate with progression (de Silva et al., 2012). Whether innate immune responses also contribute to HIV-2 viral control also remains to be explored.

One of the important specific features of HIV-2 particles is that they contain Vpx, an accessory protein that is absent in HIV-1. Vpx efficiently counteracts the restriction factor SAMHD1 by promoting its rapid degradation (Hrecka et al., 2011). SAMHD1 is a cytosolic enzyme active in resting T cells and DCs which depletes the stock of cytosolic dNTPs via its deoxynucleoside triphosphate triphosphohydrolase activity, thereby blocking the RT of lentiviruses (Hrecka et al., 2011; Laguette et al., 2011; Sunseri et al., 2011). The activity of SAMHD1 appears to be very low in activated $CD4^+$ T cells (Descours et al., 2012), intermediate in macrophages, and high in DCs (Cribier et al., 2013). Addition of Vpx in macrophages accelerates retro-transcription and nuclear integration (Bejarano et al., 2018).

Macrophage susceptibility to HIV-2 appears to be limited by low levels of surface CD4 expression that impact Env-mediated viral fusion (Chauveau et al., 2017). Primary isolates of HIV-1 and HIV-2 appear to exhibit different replication kinetics in MDMs as judged by RT activity (Marchant et al., 2006). HIV-2 viral particles are released from MDMs, with an initial burst at day 2 post-infection (p.i.), which decreases thereafter. In contrast, HIV-1 is produced in MDMs at a low but constant rate over 21 days. HIV-2 infectivity was much lower than HIV-1 when the virus was produced in MDMs whereas infectivity was similar, yet low, when the virus was produced in PBMCs (Marchant et al., 2006). Replication kinetics and viral production in MDMs, have been estimated using HIV particles carrying their own Env together with VSV-G to bypass potential restriction at the entry step, and found for HIV-2 GL-AN to be more rapid and superior to that of the HIV-1 strains tested (Hollenbaugh et al., 2016).

There is little knowledge concerning the HIV-2 cycle in macrophages. Aside from the entry step, which relies on the highly variable Env glycoprotein, differences between the rest of the HIV-1 and HIV-2 genomes may lead to differences in the viral cycle in primary macrophages. Here we used HIV-1 and -2 viruses pseudotyped with VSV-G to normalize the entry step. We show that HIV-2-infected macrophages efficiently produced new viral particles in apparently intracellular compartments. These new viral particles were poorly transmitted to T cells, likely due to the poor quality of the viral particles produced by HIV-2-infected MDMs and the low susceptibility of $CD4^+$ T cells to HIV-2. HIV-2-infected MDMs may only weakly contribute to the spread of the infection. They may, however, provide a source of cell-associated viral antigens that could stimulate the adaptive anti-viral immune response.

MATERIALS AND METHODS

Cells

Peripheral blood mononuclear cells (PBMC) were separated from plasmapheresis residues using Ficoll-Paque (GE Healthcare). Monocytes were isolated by $CD14^+$ positive selection using magnetic microbeads (Miltenyi) and differentiated into macrophages for 7 days in RPMI (Gibco, Life Technologies) supplemented with 5% fetal calf serum (FCS; BioWest), 5% human serum AB (Sigma), penicillin- streptomycin (Gibco), and 25 ng/ml macrophage colony-stimulating factor (M-CSF; ImmunoTools). $CD4^+$ T cells were isolated from PBMC by negative selection using magnetic microbeads (Miltenyi).

Cell Culture

$CD4^+$ T cells were cultured in RPMI 1640 medium, GlutaMAX complemented with FBS 10% and Penicillin/Streptomycin at 10^6 cells/mL in the presence of 5 μg/mL PHA (Lectin from *Phaseolus vulgaris* Leucoagglutinin; Sigma L2769) and 50 U/mL of IL-2 (eBioscience). On day 2 of culture, cells were washed and additionally cultured with IL-2. HEK293FT cells were cultured in DMEM medium, GlutaMAX (Thermo Fisher 61965-026) complemented with FBS 10% (Thermo Fisher 10270-106) and Penicillin/Streptomycin. GHOST X4R5 and TZM-bl cells were cultured in DMEM medium, GlutaMAX complemented with FBS 10% and Penicillin/Streptomycin. MT4C5 cells were cultured in RPMI medium, GlutaMAX complemented with FBS 10% and Penicillin/Streptomycin. All cells were cultured at 37°C with 5% CO_2 atmosphere.

Plasmids

HIV-1 NL4-3 (kindly provided by O. Schwartz, Institut Pasteur, Paris, France), HIV-1 NL-AD8 (Freed and Martin, 1995) derived from of NL4-3 with BaL Env, HIV-2 ROD9 and HIV-2 JK (both were gifts from N. Manel). The GFP viruses all harbor GFP instead of Nef: HIV-1 NL4-3 X4GFP (N. Manel), HIV-2 ROD9GFP and HIV-2 ROD9ΔEnvGFP (both kindly provided by O. T. Keppler), HIV-2 JKGFP (Silvin et al., 2017). HIV-1iGFP is internally tagged with EGFP sequence between MA and CA (Hubner et al., 2007). Similarly, HIV-2 ROD9GagiGFP was generated by inserting the EGFP sequence between MA and CA of Gag (gift of N. Manel). Vpu-Lai plasmid (kindly provided by S. Saragosti, Saint Louis Hospital) was used to generate Vpu-Cherry that was cloned into a pDONOR vector and transferred by gateway technology to pCDH-CMV-MCS-EF1-Puro (SBI bioscience). For lentiviral transduction, we also used pSIV3+ plasmid for Vpx, psPAX2 for lentiviral encapsidation and pDM2G for VSV-G pseudotyping. HIV-2 ROD9iGFP and HIV-2 Δψ (pSVRΔNBDM plasmid) (Lahaye et al., 2013) were co-transfected into HEK293FT cells to produce infectious particles.

HIV-1 and Lentiviral Production and Titration

HIV viral particles were produced by transfection of HEK293FT cells in 6-well plates with 3 μg DNA and 8 μl TransIT-293 (Mirus Bio) per well. For non-pseudotyped virus 3 μg of HIV plasmid were used. For VSV-G pseudotyped virus 0.4 μg pDM2G and 2.6 μg HIV plasmid were used. For Vpx and Vpu-Cherry lentivectors 0.4 μg pDM2G, 1 μg psPAX and 1.6 μg Vpx or Vpu-Cherry plasmid were used. For production of HIV-2*GagiGFP, we used a mix of 3 plasmids: 0.4 μg pDM2G, 1 μg pSVRΔNBDM and 1.6 μg pROD9GagiGFP. 16 h after transfection, media was removed, and fresh RPMI medium was added. Viral supernatants were harvested 36 h later, filtered at 0.45 μM, used freshly or aliquoted and frozen at −80°C. Viral titers were determined on GHOST X4R5 cells as described (Manel et al., 2010).

Drugs

Azidothymidine (AZT; Sigma) was used at 25 μM final concentration and added at time of co-culture with T cells as control or after 24 h of co-culture to avoid T-to-T cell transmission.

Flow Cytometry

Macrophages were harvested after TrypLE™ Express treatment (Gibco) and gentle scraping. Cells were fixed for 20 min in 4% paraformaldehyde (PFA), washed in PBS, and when stained, permeabilized for 30 min in PBS plus 0.2% BSA and 0.05% saponin. Infection was detected by GFP coding viruses and BST2 was detected using a coupled BST2-PE antibody (eBioscience) or IgG1-PE (eBioscience) as a control and analyzed on a FACS Verse (BD). For Vpu-Cherry expressing cells CYTOFLEX cytometer (Beckman Coulter) was used.

Recovery of Intracellular Virus

Macrophages in a 24-well plate were washed twice in PBS after supernatant collection and 400 μL of media were added and stored at −80°C. After 2 h the plate was thawed and medium was collected and centrifuged at 15,000 rpm 1 h 30 at 4°C. The pellet was resuspended in 200 μL. 100 μL were used for RNA extraction and 100 μL were diluted with 300 μL of PBS for titration into TZM-bl.

RNA Isolation, Reverse Transcription, and qPCR

At the time of collection, supernatant was collected directly and 400 μl of supernatant and 100 μL of recovered intracellular virus were lysed with 1,400 and 350 μL of lysis buffer, respectively (Macherey-Nagel). 200 pg of Luciferase control RNA (Promega) were added to each sample for absolute quantification. RNA was collected and purified using the NucleoSpin RNA kit (Macherey-Nagel) by following the manufacturer's instructions. RNA quality and quantity were verified with a NanoDrop 2000 (Thermo Scientific), and RT was performed using a high-capacity cDNA reverse transcription kit (Applied Biosystems) according to the manufacturer's instructions. qPCR was performed using SYBR green Master Mix (Roche). Primers for full length gag HIV-1 and HIV-2 were designed to be in the same part of the gag sequence with similar length, Tm and % GC (HIV-2 Forward 5′-CGGCGGAAAGAAAAAGTACA-3′ and Reverse 5′-CACCAAATGACGCAGACAGT-3′; and

HIV-1 Forward 5′-CGAGAGCGTCGGTATTAAGC-3′ and Reverse 5′-CTGAAGGGATGGTTGTAGCTG-3′) based on (Houzet et al., 2007) for gRNA quantification.

Viral Genomic RNA Quantification

Standard curves of each plasmid and Luciferase RNA control (Promega) were run for each donor and plate of qPCR. The equations from the standard curves were used to calculate absolute values for HIV gRNA copies/μL with sample normalization for RNA luciferase.

Rate of Infection on TZM-bl and Infectivity

Supernatant and recovered intracellular virus from MDMs were titrated on TZM-bl cells for 48 h using Steady-Glo Luciferase assay system (Promega) according to manufacturer's instructions. Luminescence was read on a spectrometer (FLUOstar OPTIMA). The rate of infection (AU/μL) was calculated using the slope of the linear regression of the titration. Infectivity was calculated normalizing the rate of infection by the HIV RNA copies/μ L.

Confocal Microscopy and Immunostaining

Cells were fixed for 20 min in 4% paraformaldehyde (PFA), washed in PBS, and when stained, permeabilized for 30 min in PBS plus 0.2% BSA and 0.05% saponin. Gag was stained with H183-H12-5C hybridoma (mouse IgG1, NIH) or p24 (goat polyclonal, Abcam) only when co-stained with CD36. For cellular proteins CD44 (rat, Abcam), CD9 (rabbit, Santa Cruz), CD36 (mouse IgG1, StemCell), CD81 (mouse IgG2a, Abcam) and Lamp1 (rabbit, Abcam) were used. For secondary antibodies goat anti-IgG1 A546, goat anti-IgG2a A647, donkey anti-rabbit A488, donkey anti-goat A488, chicken anti-mouse A647, donkey anti-rabbit Cy3, donkey anti-mouse A488 and donkey anti-rat A647 were used (Life technologies).

For the Gag co-staining with different markers by immunofluorescence, single plane images (pixel size 70 nm) were acquired using an inverted confocal microscope (Zeiss, LSM780) equipped with a 40× oil immersion objective (NA = 1.3), an argon laser and three laser diodes (405, 546, and 633 nm) when required.

For the 3D % of Gag signaling measurement, Z stacks (pixel size 70 nm, Z step = 0.3 μm) were acquired using an inverted confocal microscope (Leica DMi8, SP8 scanning head unit) equipped with a 63× oil immersion objective (NA = 1.4) and four laser diodes (405, 488, 546, and 633 nm).

Image Analysis

Image processing and analysis were performed using Fiji software (Schindelin et al., 2012). Analysis of confocal images was performed by different approaches. Line scans: the same line scan profile was applied to the different channels, profiles were performed using line profile function and normalized to their highest value before plotting the data on overlay graphs.

For the analysis of the enrichment of the different markers within VCC and cytoplasm, VCCs were segmented by applying a threshold on the Gag channel. Cytoplasm was segmented by applying a threshold on the CD44, CD36, or CD81 channel, corrected manually and subtracting the nucleus obtained after applying a threshold on the DAPI channel. The ratio between the MFI inside the VCC versus the cytoplasm for each channel was computed.

Pearson coefficients between the CD44 channel image and the Gag channel image were computed using coloc2 plugin inside the cytosol and VCC. The same process was applied for the analysis of Gag/Lamp1 co-distribution.

For the 3D volumes measurement, 3D masks were obtained for the cytoplasm, the nucleus, and the compartments by applying threshold, respectively, on CD44 channel, DAPI channel and p24 channel. Masks were corrected or adjusted manually when necessary. The volume of each masks and their GFP intensities were then measured. 3D reconstructions were achieved using Volume Viewer plugin and the 3D masks of the Fiji software.

Electron Microscopy

Cells were fixed in 2% glutaraldehyde in 0.1 M cacoldylate buffer, pH 7.4 for 1 h, post-fixed for 1 h with 2% buffered osmium tetroxide, dehydrated in a graded series of ethanol solution, and then embedded in epoxy resin. Images were acquired with a digital camera Quemesa (SIS) mounted on a Tecnai Spirit transmission electron microscope (FEI Company) operated at 80 kV. Density of viral particles was determined as viral particles/μm^2 within VCC. Measurement of VCC area was done using iTEM analySIS software (Soft Imaging Systems).

Macrophage-to-T Cell Transmission/MT4C5

For Macrophage-to-T cell transmission, MDMs in 96-well plate and 24-well plate were infected with VSV-G–pseudotyped HIV-1 NL4.3GFP, HIV-2 ROD9GFP, and HIV-2 JKGFP at different MOIs, washed extensively 3 days later, and received 7.5×10^5 $CD4^+$ T lymphocytes/well in the 96-well plate. MDMs on 24-well plate were harvested for the measurement of infected cells by flow cytometry. The $CD4^+$ T lymphocytes were purified by negative selection (Miltenyi Biotec) from heterologous PBMCs that had been activated 48 h before in RPMI, 10% FCS, 2.5 μg/ml PHA-L, and 30 U/ml IL2. 25 μM AZT was added at 0 h (as a negative control) or 24 h after the beginning of the co-cultures. At 48 h, $CD4^+$ T cells were collected, washed and fixed with 4% PFA, permeabilized, stained with PE-Cy7 anti-CD3 (BD), and analyzed on a FACS Verse (BD).

For Macrophage-to-MT4C5 cell transmission, MDMs were infected 96-well plate and 24-well plate with VSV-G–pseudotyped HIV-1 NL4.3GFP, HIV-2 ROD9GFP, HIV-2 JKGFP, and HIV-2ΔEnv ROD9GFP at MOI 1.5, washed extensively 8 h later and at day 3, when received 7.5×10^5 MT4C5 cells/well in the 96-well plate. MDMs on 24-well plate were harvested for

% of infected cells, and supernatant was harvested for gRNA and infectivity quantification. 25 μM AZT was added at 24 h after the beginning of the co-cultures. At 48 h, MT4C5 cells were collected, washed and fixed with 4% PFA and analyzed on a FACS Verse (BD). Data were analyzed using FlowJo v10 and Prism v8 for Mac (GraphPad).

Statistics

Data were analyzed using Prism v8 for Mac (GraphPad). Tests for statistical significance were chosen accordingly to the data and assuming non-parametric distribution. Applied tests are specified for each figure in the legend.

RESULTS

HIV-2 Infection and Production in Primary Macrophages

We used HIV-1 and -2 viruses encoding GFP in place of Nef to quantify the rate of infection in MDMs, independently of antibodies which may have differential affinity for HIV-1 and -2 proteins. The rate of infection determined by assays based on the RT activity of both viruses was not considered because of the viruses' differential catalytic activity and sensitivity to inhibitors (De Clercq, 1993; Achuthan et al., 2017). VSV-G pseudotyped HIV-1 NL4.3GFP, HIV-2 ROD9GFP, and HIV-2 JKGFP were produced in HEK293FT cells by transfection and titrated on GHOST reporter cells for use at similar MOIs on MDMs (**Figure 1A**). Infection rates were consistently lower for HIV-1 than HIV-2 (**Figures 1B,C**). This likely resulted from the presence of Vpx in HIV-2 particles, which counteracts SAMHD1 activity. As previously shown (Hrecka et al., 2011; Sunseri et al., 2011), the rate of MDM infection by HIV-1 increased roughly 10-fold when the virus was complemented with Vpx (**Supplementary Figure S1**), showing that our preparations of HIV-1 were functional. Direct comparison of Gag amounts by flow cytometry or immunoblot was not reliable due to differences in antibody affinity for HIV-1 and -2 proteins. To accurately follow viral production by MDMs infected with the different viruses at three MOIs, we quantified HIV RNA copies at both the intra- and extracellular levels after 3 days of infection (**Figures 1D,E**). HIV-1-infected MDMs released increasing amounts of viral RNA copies in the supernatant as a function of the MOI (**Figure 1D**). HIV-2 JKGFP-G-infected MDMs released similar amounts of viral RNA despite their higher infection rates. Levels of extracellular viral RNA were very low in ROD9GFP-G-infected MDMs (**Figure 1D**). However, at the intracellular level, HIV-2 ROD9GFP-G- and HIV-2 JKGFP-G-infected MDMs contained the highest amounts of viral RNA (**Figure 1E**).

To estimate the level of cell-associated virus, we calculated the ratio of intracellular to total viral RNA copies (**Figure 1F**). HIV-1 NL4.3GFP and HIV-2 JKGFP exhibited similar low ratios whereas the ratio was higher for HIV-2 ROD9GFP, reflecting its low release from MDMs. We concluded that both HIV-2 strains contained high intracellular concentrations of viral RNA despite their differences in viral release.

HIV-2 Is Produced and Stored in HIV-1-Like Virus-Containing Compartments

To determine where viral production occurred in HIV-2-infected MDMs, we first analyzed the intracellular distribution of the viral Gag protein by immunofluorescence. Here we used VSV-G pseudotyped WT viruses and extended our analyses to R5 virus HIV-1 NLAD8, as HIV-2 JK is also R5 tropic whereas both HIV-1 NL4.3 and HIV-2 ROD9 are X4 tropic. Confocal microscopy revealed the presence of punctate structures containing high amounts of Gag in MDMs infected with HIV-1 or -2 (**Figure 2A**). Line scan profiles through Gag^+ containing compartments showed the co-enrichment of CD44 and CD9 for the four viral strains in those structures (**Figure 2B**). CD44 staining was intense at the plasma membrane and dimmer intracellularly where it was associated with Gag mainly in the punctuate structures (**Figures 2A,B**). Pearson coefficient analysis of the co-distribution of both markers in the cell showed only partial co-localisation (**Figure 2F**). The Gag-containing structures were free of Lamp1 (see **Supplementary Figure S2A** and **Figure 2G**). We also estimated the level of enrichment of CD44, CD9, and CD36 by measuring their staining intensities in the cytosol versus in the Gag^+ structures, and observed an enrichment in all conditions for the three markers (**Figures 2C–E**). We extended these quantifications to include CD81 and more donors comparing HIV-1 NLAD8 and HIV-2 ROD9 and obtained similar results (**Supplementary Figures S3A–C**). Similar staining distributions were also observed at day 7 p.i. (**Supplementary Figure S2B**). We concluded that Gag concentrated into $CD44^+CD9^+CD36^+CD81^+Lamp1^-$ compartments in MDMs infected by the HIV strains used. Such composition is typical of VCCs previously described in HIV-1-infected MDMs (Pelchen-Matthews et al., 2003; Deneka et al., 2007; Jouve et al., 2007; Bèrre et al., 2013). These findings suggest that in MDMs, like HIV-1, both HIV-2 strains hijack these compartments for their assembly.

Gag Is Almost Absent From the Cytosol but Concentrated in VCCs in HIV-2-Infected Macrophages

Gag staining in HIV-2-infected MDMs appeared to be mainly found in punctate structures that were likely to be VCCs (**Figure 2A**). In contrast, HIV-1 Gag accumulated in VCCs and was also present in the cytosol (**Figure 2A**). Quantification on confocal sections of Gag signal present in the cytosol, in VCC and their ratio (**Figures 3A–C**, respectively) confirmed this striking difference between HIV-1 and -2 Gag distribution that was observed at day 3 p.i. (**Figures 2A**, **3A–C**) and persisted to day 7 p.i. (**Supplementary Figure S2B**). Quantification on larger number of MDMs from different donors confirmed these differences in Gag distribution (**Supplementary Figure S4A**). To better show the differences in Gag localisation, we generated z projections of confocal z-stacks of infected MDMs to reconstruct in 3D the Gag^+ compartments, i.e., the VCC (see z projections in **Figure 3D**). Analysis of the Gag signal distribution, shown in

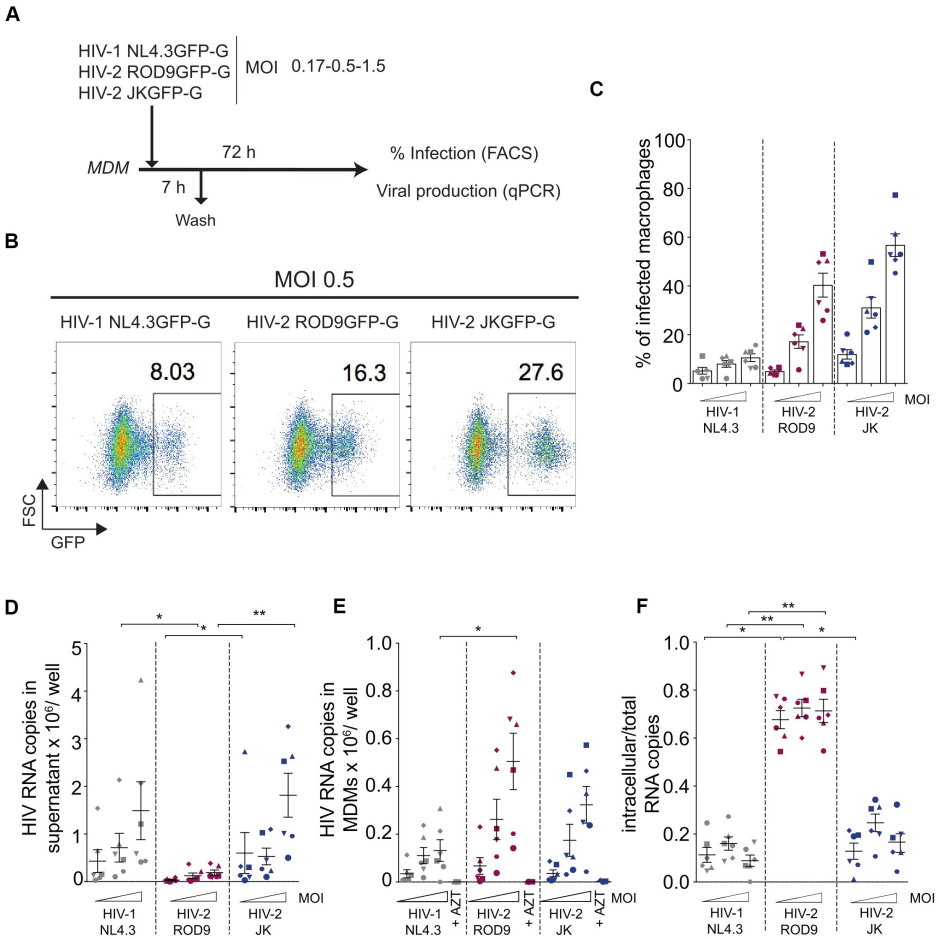

FIGURE 1 | HIV-2 infection and production of MDMs. **(A)** Outline of the experiment. Monocyte-derived macrophages were differentiated for 7 days with M-CSF (MDMs), infected with the indicated viruses for 7 h at different MOIs and harvested at 3 dpi for analysis of GFP expression by flow cytometry and viral genomic RNA quantification. **(B)** Representative dot plot analyses of infected MDMs with percentages of GFP^+ cells indicated in the plots. **(C)** Percentages of GFP^+ MDMs infected with the indicated viruses at 3 dpi. **(D)** Viral release in the supernatant and **(E)** Intracellular viral content at 3 dpi of MDMs evaluated by RT-qPCR. **(F)** Ratio of intracellular viral copies over total viral copies produced by infected MDMs. $n = 6$ from 3 independent experiments, individual data (each symbol representing one MDM donor across the panels) displayed with means ± standard deviations (SD). *P*-values were calculated using non-parametric Friedman paired test. *P*-values lower than 0.05 were considered as significant ($*p < 0.05$, $**p < 0.01$, $***p < 0.001$, $****p < 0.0001$).

pseudo-colors to visualize very low levels, confirmed that Gag was mostly absent from the cytosol in HIV-2-infected MDMs and concentrated in VCCs (**Figure 3D**). This conclusion was further supported by quantification of the Gag signal present in VCCs/in the whole cell, in 3D stacks of images of HIV-infected MDMs (**Figure 3E**).

To rule out that the differential distribution of HIV-1 and HIV-2 Gag was due to differential affinity of the H183-H12-5C mAb used for the cytosolic Gag forms, we infected MDMs with HIV strains internally tagged with GFP. The GFP was inserted between the matrix and capsid within the p55 Gag precursor between two protease sites (see Hubner et al., 2007 and methods). The GFP signal and Gag staining were co-distributed in HIV-1iGFP- and HIV-2*iGFP-infected MDMs (**Supplementary Figure S4B**), confirming the differential distribution of Gag.

The addition of Vpx to HIV-1 NL4.3GFP-G increased the infection rate of MDMs as expected (**Supplementary Figure S1A**), but did not modify Gag distribution (**Supplementary Figures S4C,D**). These data suggest that both HIV-2 strains ROD9 and JK Gag were more efficiently recruited to VCCs after synthesis in the cytosol than HIV-1 Gag.

Ultrastructural Analysis of VCCs From HIV-2-Infected Macrophages

We analyzed ultrathin sections of HIV-2-infected macrophages by electron microscopy to further characterize the morphology of their VCCs (**Figure 4**). VCCs from MDMs infected with HIV-1 NLAD8-G or HIV-2 ROD9-G or HIV-2 JK-G exhibited highly similar morphologies. In all cases we observed viral budding profiles at the VCC limiting membranes (see arrowheads), revealing the production of new virions. The budding process occurs away from the cytosol, at the limiting membrane of the VCC, and new virions accumulate in the VCC lumen.

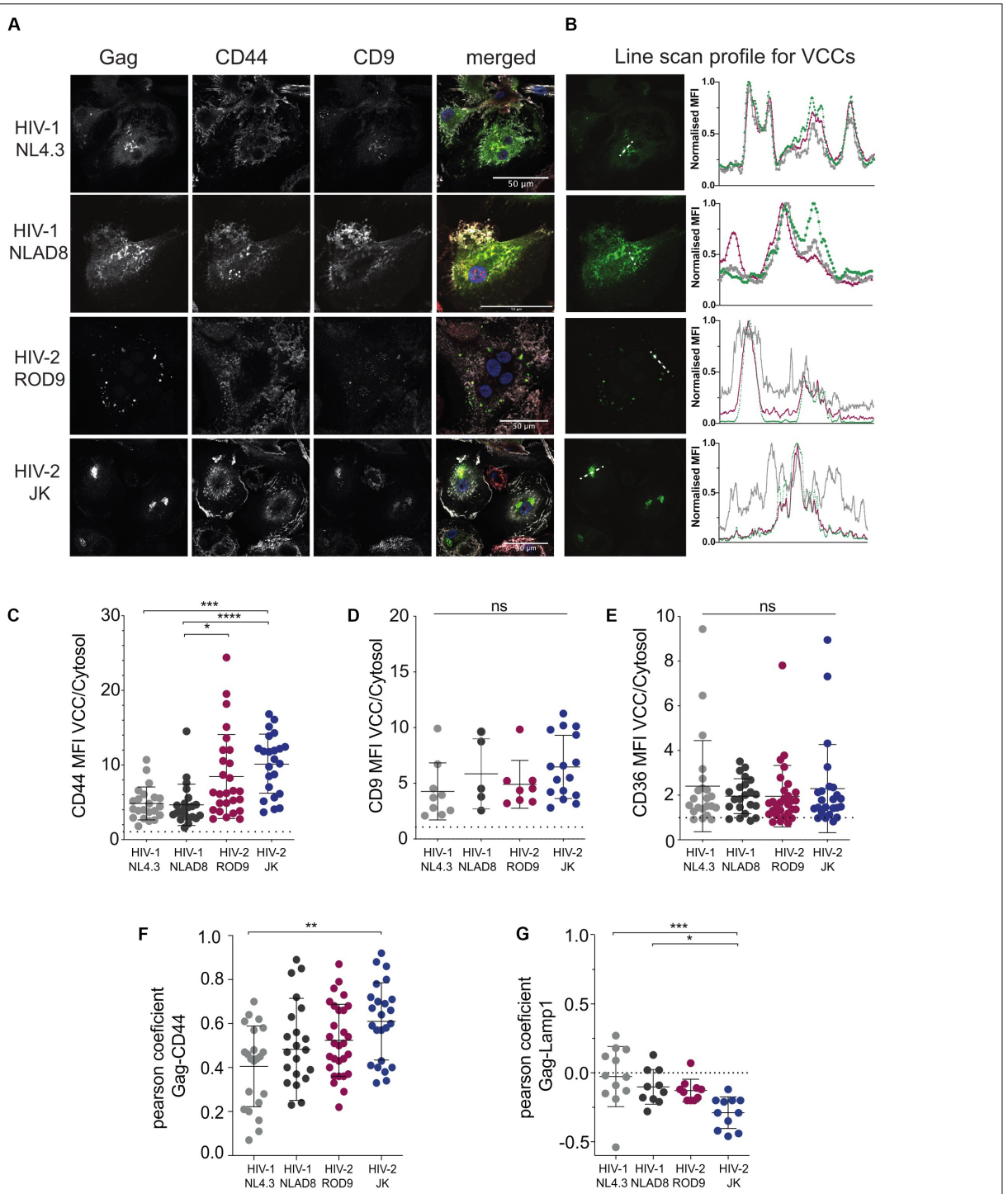

FIGURE 2 | HIV-2 Gag localizes in Virus-Containing Compartments in primary human MDMs. **(A)** MDMs were infected for 3 days with the indicated viruses, all VSV-G-pseudotyped. Samples were stained for the indicated markers by immunofluorescence. Representative confocal sections are presented from at least 6 donors. **(B)** Line intensities profiles for all the markers **(A)**. Profiles were performed on the white dotted lines shown on the Gag images. Intensities profiles were normalized to highest value for each marker. Green line corresponds to Gag, gray to CD44 and red to CD9. **(C–E)** Quantification of each marker enrichment in VCCs calculated as the ratio MFI present in VCCs over the one present in the cytosol on confocal sections. VCC and cytosol were segmented by masks on Gag and CD44 staining, respectively (see section "Materials and Methods"). **(F)** Analysis of the co-distribution between Gag and CD44 and **(G)** between Gag and Lamp1 on confocal sections by measurement of the Pearson coefficient. Each dot represents a cell. *P*-values were calculated using Kruskal–Wallis non-parametric test with Dunn's correction for multiple comparison. *P*-values lower than 0.05 were considered as significant (*$p < 0.05$, **$p < 0.01$, ***$p < 0.001$, ****$p < 0.0001$).

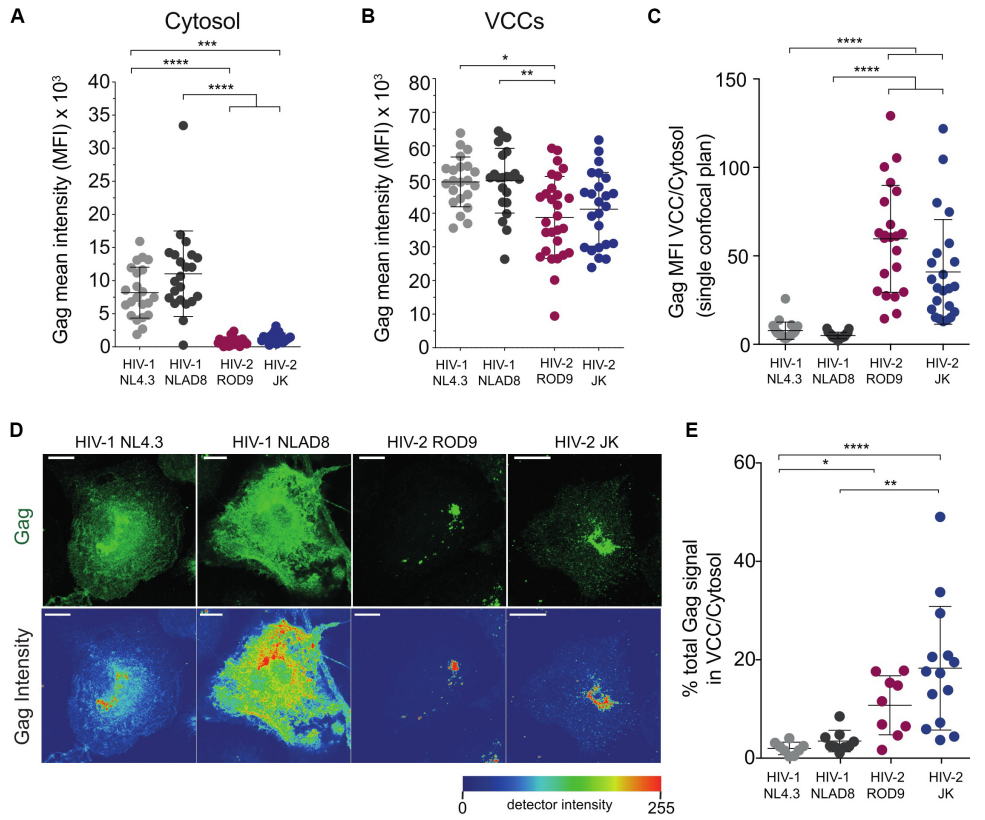

FIGURE 3 | Gag is concentrated in the viral-containing compartment of HIV-2-infected MDMs. **(A,B)** Gag MFI in the cytosol **(A)** and in the VCCs **(B)**. A macro was used to build masks that delimited the VCCs based on Gag and the Cytosol based on CD44 plasma membrane staining (see section "Materials and Methods"). **(C)** Gag enrichment in the VCCs calculated as the ratio of the MFI in VCCs **(B)** over the MFI in the cytosol **(A)** on confocal sections. **(D)** Representative Z projections of a stack of images obtained by confocal microscopy. Images displayed on the second row represent intensity maps for Gag expression using pseudo-color. Bar = 10 μm. **(E)** Z stacks of infected MDMs were used to obtain 3D masks and to determine the % of Gag signal present in VCCs over Gag signal present in the rest of the cells. Each dot represents a cell. Data presented from a representative donor from at least 6. *P*-values were calculated using Kruskal–Wallis non-parametric test with Dunn's correction for multiple comparisons. *P*-values lower than 0.05 were considered as significant (*$p < 0.05$, **$p < 0.01$, ***$p < 0.001$, ****$p < 0.0001$).

The VCCs contained mature and immature viral particles in their lumen. The presence of mature (with the electron dense capsid visible inside) and immature (with the electron dense Gag precursor at the periphery and an electron lucent zone at the center) particles revealed that they were able to mature. Quantification of the viral density in the lumen of the VCCs did not reveal any significant differences among the three types of infected MDMs (**Figure 4D**). We observed higher numbers of compartments per section in HIV-2-infected MDMs, probably reflecting the higher rate of infection than seen with HIV-1 (see number of dots per condition in **Figure 4D**).

One of the important characteristics of MDM VCCs is their connection to the extracellular medium, which can be witnessed at the ultrastructural level using the membrane impermeant dye ruthenium red (RR) (Deneka et al., 2007; Jouve et al., 2007). The RR dye decorates membranes with a characteristic electron dense staining. We performed an ultra-structural analysis of HIV-2-infected MDMs exposed to RR just before fixation and inclusion (**Figures 4E,F**). It revealed that the limiting membranes of VCCs from MDMs infected by both strains of HIV-2 were stained by RR as well as the membranes of the intralumenal viral particles.

These results show that HIV-2 assembled, budded and accumulated in VCCs similarly to those present in HIV-1-infected MDMs. The main difference was the paucity of cytosolic Gag in HIV-2- versus HIV-1-infected cells.

HIV-2-Infected Macrophages Poorly Transmit the Infection to Activated Primary CD4$^+$ T Cells

The addition of activated T cells to HIV-1-infected MDMs has been proposed to promote polarization of VCCs and transfer of their viral contents to T cells (Gousset et al., 2008). To evaluate whether activated T cells could stimulate HIV-2-infected MDMs to release and transfer their intra-VCC viral stocks, we performed MDM-to-T cell transmission assays using HIV-1 NL4.3GFP-G and HIV-2 ROD9GFP-G, both are X4-tropic HIVs (**Figure 5A**). Infection of MDM at various MOIs yielded similar or higher rates of infection for HIV-2 ROD9GFP-G than HIV-1 NL4.3GFP-G (**Figures 5B,C**). Although HIV-1-infected MDMs efficiently

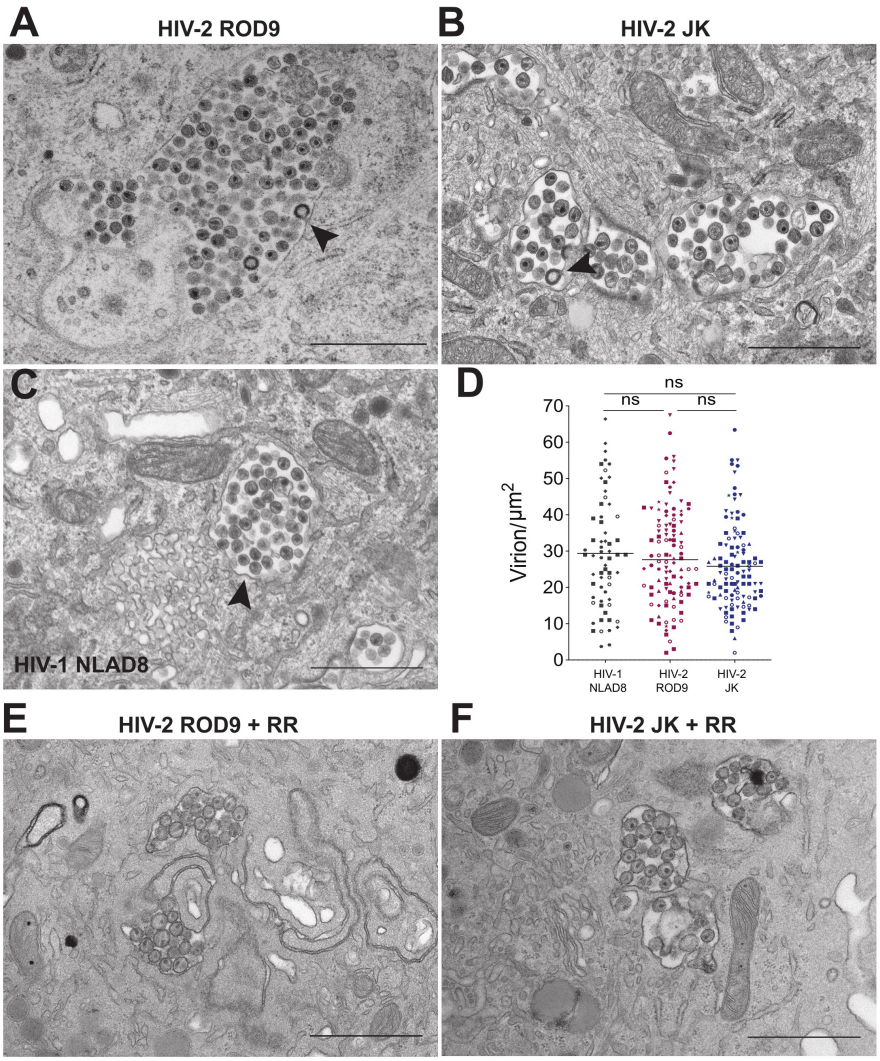

FIGURE 4 | HIV-2 assembles and buds in *bona fide* VCC of MDMs. **(A–C)** MDMs infected with the indicated pseudotyped viruses for 3 days were fixed and processed to perform electron microscopy (see section "Materials and Methods"). A representative epon section of infected MDM from 5 donors is presented. Arrowheads point to nascent viral buds. **(D)** Quantification of the density of viral particles present within the VCCs calculated for each epon sections of infected MDMs. Each dot represents a VCC. Bars represent Grand means. Donors: NLAD8 $n = 4$, ROD9 $n = 7$, and JK $n = 5$. **(E,F)** MDMs infected with the indicated pseudotyped viruses for 3 days were fixed in the presence of Ruthenium Red and processed to perform electron microscopy. *P*-values were calculated using Kruskal–Wallis non-parametric test with Dunn's correction for multiple comparison. *P*-values lower than 0.05 were considered as significant ($^{*}p < 0.05$, $^{**}p < 0.01$, $^{***}p < 0.001$, $^{****}p < 0.0001$).

transmitted the virus to T cells, transmission by HIV-2-infected MDMs was very low (**Figures 5D,E**).

HIV-2 Particles Produced by MDM Are Poorly Infectious

The low transmission rates prompted us to evaluate the quality of the viruses produced by HIV-1- and HIV-2-infected MDMs at day 3 p.i. Viral production was titrated on the TZM-bl reporter cell line and normalized by quantification of gRNA. The GHOST and TZM-bl reporter cell lines allow comparable titrations, albeit TZM-bl cells are more sensitive (**Supplementary Figure S5A**). MDMs were infected with either HIV-1 NL4.3GFP-G, HIV-2 JKGFP-G, HIV-2 ROD9GFP-G or with HIV-2ΔEnv ROD9GFP-G as a negative control for infectivity (**Figure 6A**). Infection rates of both HIV-2 strains were much lower than that of HIV-1, and were null for HIV-2ΔEnv as expected (**Figures 6B,C**). Combined with the estimation of the viral content of the supernatant (**Figure 6D**), the infectious capacity of the HIV-2 viruses produced by MDMs was very low (**Figures 6E,F**): less than 50% of the infectivity of HIV-1 for HIV-2 ROD9GFP, and 20% for HIV-2 JKGFP.

Our data suggest that viral particles produced by HIV-2-infected MDMs possess reduced infectivity compared to HIV-1, as judged on TZM-bl reporter cells. In addition, HIV-2 WT particles produced by HEK293FT cells infected $CD4^{+}$ T cells less

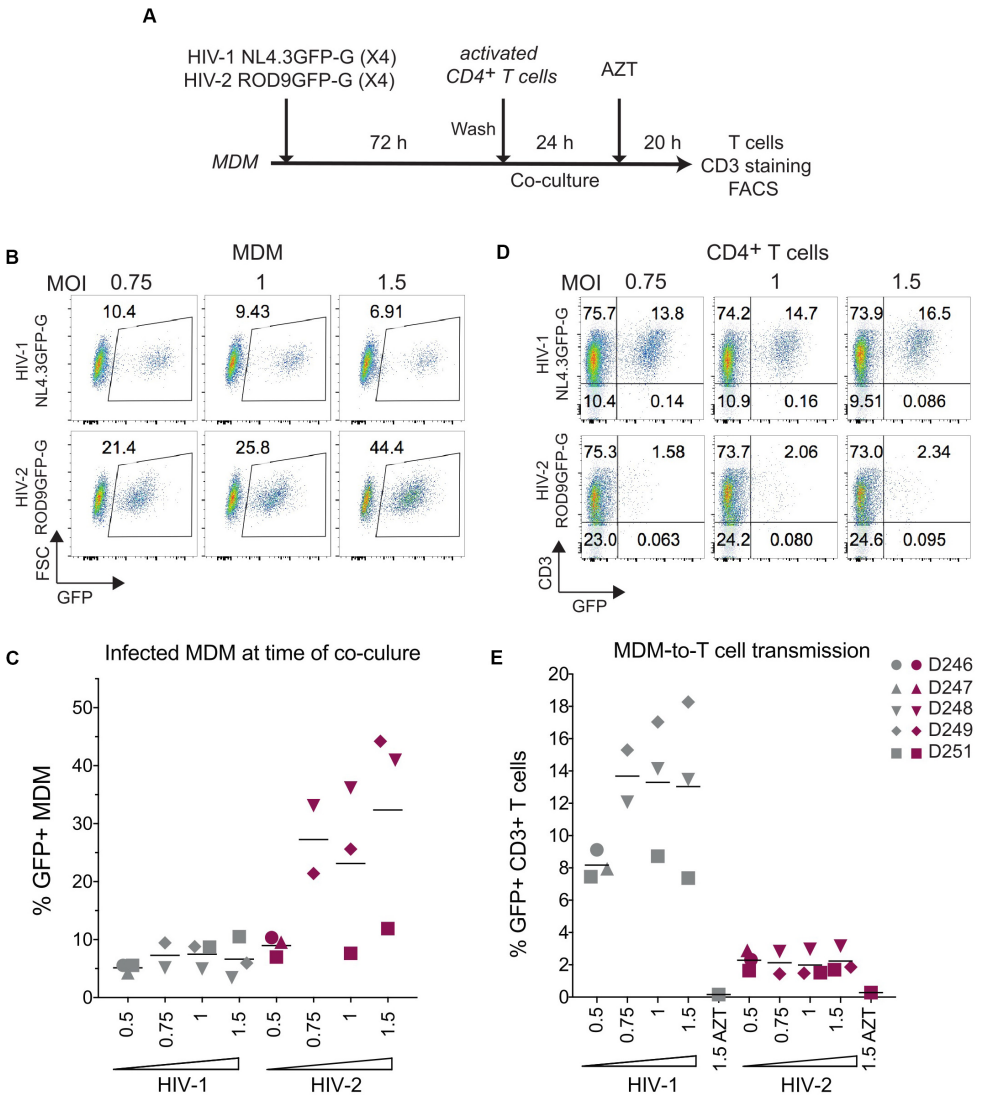

FIGURE 5 | HIV-2 transmission from infected MDM to activated CD4$^+$ T cells is inefficient. **(A)** Macrophage-to-T cell transmission, outline of the experiment. **(B)** Representative dot plot of GFP expression of HIV-infected MDMs analysed at 3 dpi by flow cytometry. Percentages of GFP$^+$ cells are indicated in the gates. **(C)** Percentages of GFP$^+$ MDMs at 3 dpi as in **(B)**, *n* = 5 donors from 3 independent experiments, bars representing the mean. **(D)** Representative dot plots of GFP and CD3 expression at the end of the 44 h co-culture. **(E)** Percentages of CD3$^+$GFP$^+$ T cells after co-culture with infected MDM as in **(D)**, *n* = 5 donors from 3 independent experiments, bars representing the mean.

well compared to HIV-1 (**Supplementary Figure S5**), even when compared at the same GHOST-determined MOI (see vertical boxes **Supplementary Figure S5C**). Low HIV-2 infection rates of T cells observed in the transmission experiments appear to result from the low infectivity of the HIV-2 particles produced by infected MDM combined with the low susceptibility of CD4$^+$ T cells to HIV-2.

BST2 Regulation in HIV-Infected Macrophages

The low amounts of HIV-2 ROD9 released and the low infectivity of HIV-2 particles produced by MDMs may result from partial down-regulation of the restriction factor BST2/Tetherin. BST2 affects viral release and infectivity of newly produced viral particles (Neil et al., 2007). It is counteracted by the small accessory HIV-1 protein Vpu by promoting its removal from the plasma membrane in T cells and further degradation (Neil et al., 2008). Vpu is absent from HIV-2 but its Env glycoprotein can sequester BST2 into the *Trans*-Golgi Network, as shown so far only in HeLa cells (Le Tortorec and Neil, 2009; Hauser et al., 2010).

HIV-2 ROD9 possesses an Env glycoprotein with a short cytoplasmic tail and carries point mutations at sites described to be important for BST2 counteraction (Bour and Strebel, 2003). Nevertheless, HIV-2 ROD9-infected MDMs were able to downregulate BST2 as determined by flow cytometry on fixed and permeabilized cells, although BST2 downregulation was stronger

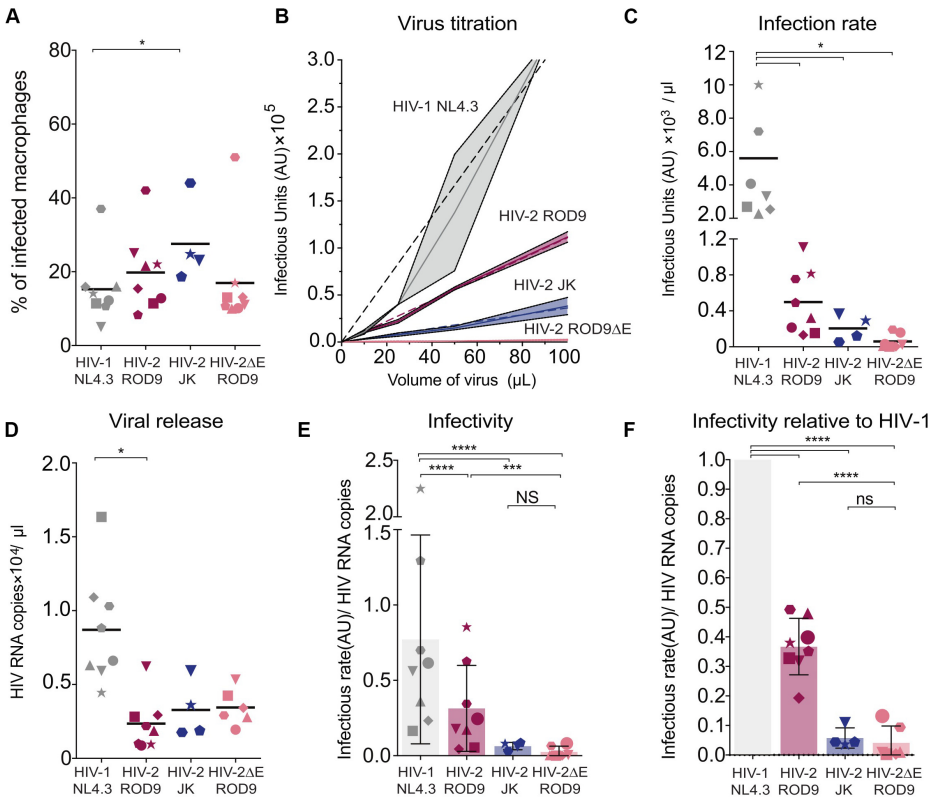

FIGURE 6 | Infected MDMs produce poorly infectious HIV-2 particles. MDMs were infected with the indicated viruses. MOIs were estimated on GHOST reporter cells and adjusted to reach similar infection rates in MDMs. *n* = 8 donors from 5 independent experiments, with bars representing the mean. Each symbol represents an individual donor across all the panels. **(A)** At 3 dpi, rates of MDMs infection were determined by flow cytometry. Percentages of infected MDM, i.e., GFP^+, at 3 dpi. **(B)** Representative virus titration on the TZM-bl reporter cell line. Serial dilutions of supernatant from each type of HIV-infected MDM were added on TZM-bl cells. Infection rates (Infectious Units/µL) were determined by calculation of the slope of the titration curve built with technical replicates. **(C)** Infection rates determined as in **(B)** with MDMs from the 8 donors. **(D)** Viral RNA copies released at 3 dpi in the supernatant of HIV-infected MDMs evaluated by RT-qPCR. **(E)** Infectivity of the released viral particles, calculated as rate of infection and normalized by genomic HIV RNA copies. **(F)** Infectivity normalized to HIV-1 for each donor. *P*-values were calculated using paired Mixed-effect analysis with Geisser–Greenhouse correction for multiple comparison test. *P*-values lower than 0.05 were considered as significant (*$p < 0.05$, **$p < 0.01$, ***$p < 0.001$, ****$p < 0.0001$).

with HIV-1 and HIV-2 JK (**Figure 7A**). We checked that HIV-2 JK Env possesses a complete cytoplasmic tail and none of the mutations described to compromise BST2 counteraction. While both HIV-2 strains downregulated BST2 expression, HIV-2 ROD9ΔEnv did not (**Figure 7A**). We concluded that HIV-2 infection of MDMs was accompanied by an Env-mediated downregulation of total BST2 expression.

To better counteract BST2, we exposed MDMs to both HIV-2 and lentivirus carrying HIV-1 Vpu fused to mCherry to induce a HIV-1-like BST2 downregulation. Vpu-Cherry was expressed in 84% (for HIV-2 ROD9) and 77% (for HIV-2 JK) of infected MDMs (**Figure 7B**). Expression of Vpu-mCherry reduced BST2 levels, which became similar to or lower than those observed in HIV-1- infected MDMs (**Figure 7A** and **Supplementary Figure S6A**). However, Vpu-Cherry expression did not significantly impact on the infectivity of the particles produced by MDMs (**Figure 7C** and **Supplementary Figures S6B,C**), nor did it affect MDM-to-T cell transmission using a $CD4^+$ T cell line expressing both HIV co-receptors (**Figure 7D**).

We concluded that the reduced release for ROD9 and weak infectivity of both HIV-2 strains produced by MDMs cannot be or could only marginally be ascribed to BST2-mediated restriction.

DISCUSSION

The involvement of macrophages in the pathophysiology of HIV-1 infection has recently been highlighted (Honeycutt et al., 2016, 2017; Araínga et al., 2017). Infected macrophages have even been found in individuals under cART in the liver and the urethra (Kandathil et al., 2018; Ganor et al., 2019). HIV-1-infected macrophages are likely to fuel the maintenance of the viral reservoir in infected patients under anti-retroviral therapy due to their resistance to the cytopathic effect of the virus, their capacity to store infectious particles and their localization in tissues. In contrast to HIV-1, knowledge concerning the relationship between macrophages and HIV-2 is scarce. We undertook the present study using an *in vitro* model of primary human MDMs and focused on the post-entry steps to evaluate whether HIV-2

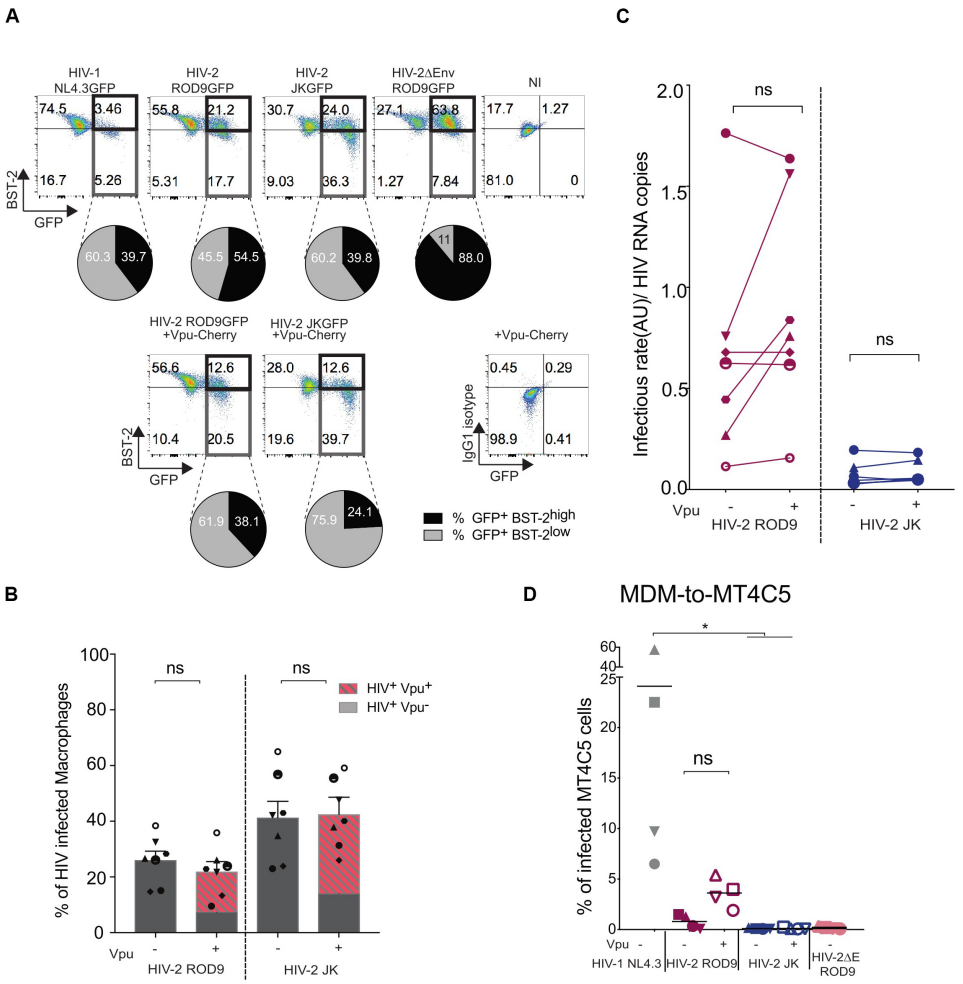

FIGURE 7 | Vpu-induced downregulation of BST2 does not rescue infectivity of the viral particles produced by HIV-2-infected MDMs. MDMs were infected with the indicated HIV or not (NI = non-infected) supplemented with lentiviral particles encoding the fusion protein Vpu-Cherry. At 3 dpi, cells were recovered, fixed and stained for BST2. **(A)** Representative dot plot of BST2 versus GFP expression. GFP^+BST2^{low} cells are boxed to ease comparisons. Pie charts represent BST2 expression within the infected GFP^+ cells. Isotype control staining is shown at the bottom right. **(B)** Rates of infection were evaluated by measuring the percentage of GFP^+ MDM exposed or not to Vpu-Cherry lentiviral particles. Percentages of GFP^+ cells and of GFP^+Vpu^+ (in dashed red) are displayed. Each symbol represents a donor (n = 7 from 4 independent experiments). Bars represent the mean ± SEM. **(C)** Infectivity of the released viruses +/– Vpu, calculated as rate of infection/HIV RNA copies measured as **Figure 5E** (see also **Supplementary Figure S5**). For **(B,C)** P-values were calculated using matched-pairs Wilcoxon non-parametric test. P-values lower than 0.05 were considered as significant. **(D)** Addition of Vpu to HIV-2 ROD9-infected MDMs partially rescues transmission to MT4C5 cells. Percentages of GFP^+ MT4C5 cells, which is a $CD4^+CCR5^+CXCR4^+$ T cell line, after co-culture with MDMs infected with indicated HIV +/– lentiviral particles encoding Vpu-Cherry. n = 4 from 2 independent experiments with bars representing the mean. P-values were calculated using paired Friedman non-parametric multiple comparison test. P-values lower than 0.05 were considered as significant (*$p < 0.05$, **$p < 0.01$, ***$p < 0.001$, ****$p < 0.0001$).

possesses any intrinsic features that could contribute to its low pathogenicity and better immune control.

We focused on the late stages of the HIV-2 viral cycle in macrophages by normalizing the entry step by pseudo-typing viral particles with VSV-G. All our results were obtained with only two HIV-2 strains and therefore might not be generalized to other HIV-2 strains that are genetically diverse (Gao et al., 1994; James et al., 2019). Our data show that upon entering macrophages HIV-2 replicated better than HIV-1, probably due to the presence of Vpx in HIV-2 that efficiently counteracts SAMHD-1 restriction. HIV-2 assembled, bud and accumulated in the same apparently intracellular compartments, named VCCs, as HIV-1. The composition and the morphology of the VCCs appeared to be similar for both viruses based on the presence of specific markers and our ultrastructural analyses. Comparative proteomic analysis of the HIV-1 and HIV-2 particles produced by macrophages would be informative as the composition of the viral membrane directly reflects that of the VCC limiting membrane (see Chertova et al., 2006).

Virus-containing compartments pre-exist in uninfected MDMs (Deneka et al., 2007; Bèrre et al., 2013) and are thought to originate from specific areas of the plasma membrane which are internally sequestered (Pelchen-Matthews et al., 2012). As a result, they often stay connected to the plasma membrane via

microchannels (Deneka et al., 2007) or conduits (Bennett et al., 2009), which are too narrow for the virions that they contain to access the external medium. This access is in line with the internal neutral pH observed in the lumen of the VCC (Jouve et al., 2007). These connections allow small molecules, e.g., dextrans or dyes, such as ruthenium red (Deneka et al., 2007; Jouve et al., 2007; Gaudin et al., 2013), to rapidly access the lumen. Here we have shown at the ultra-structural level that VCCs from HIV-2 ROD9- or HIV-2 JK-infected MDMs were accessible to the ruthenium red dye, exhibited viral budding profiles and contained both immature and mature virions. These VCCs exhibited features similar to VCCs from HIV-1-infected MDMs, including their general morphology and connections with the extracellular milieu.

One striking difference between HIV-1- and HIV-2-infected MDMs concerned the intracellular distribution of the Gag precursor. HIV-2 Gag was almost absent from the cytosol and concentrated solely in VCCs, whereas HIV-1 Gag was clearly present in both locations. Quantification on 2D confocal sections and 3D reconstitutions confirmed this difference. Several hypotheses can explain these observations. Saturation of docking sites for Gag at the limiting membrane of VCC only in the case of HIV-1 Gag would account for its more abundant presence in the cytosol. Gag binding to the VCC limiting membrane probably depends on several parameters including its concentration, level of oligomerization and thus its affinity for the $PI(4,5)P_2$ rich VCC membranes (Ono et al., 2004). Our data may alternatively reflect that once HIV-2 Gag is synthesized in the cytosol, it is rapidly targeted to the limiting membrane of the VCC. Two regions of the Gag precursor have been described as being key for the anchoring of Gag to the PM in T cells: the highly basic region and amino acids 84–88. The basic region comprises amino acids 16–31 (Ono, 2010) and is conserved between HIV-1 NL4.3, HIV-2 ROD9, and HIV-2 JK with only a charge change mutation at position 28 from Lys to Gln between HIV-2 and HIV-1. The 84–88 region is also different between the two viruses with a major change of Cys in HIV-2 to Ala in HIV-1 at position 84. How these few amino acid changes may impact Gag trafficking and anchoring to membranes and whether this difference in localization of Gag represents an intrinsic feature of the Gag proteins or results from the action of another viral gene product represent exciting questions for future studies.

HIV-2-infected MDMs contained high amounts of intracellular virions as seen by EM and quantification of viral RNA present in cell lysates. HIV-2 ROD9-infected MDMs released low amounts of viral particles while HIV-2 JK- and HIV-1 NL4.3-infected MDMs released similarly higher amounts. Whether the viral release from HIV-1-infected MDMs is regulated and inducible is still elusive. One of the few documented stimuli is eATP which rapidly induces viral release through a P2X7R-dependent mechanism that remains in large parts elusive (Graziano et al., 2015).

It has also been proposed that activated $CD4^+$ T cells can promote the transfer of virions from VCCs of HIV-1-infected MDMs to T cells via virological synapses (Gousset et al., 2008). However, addition of activated $CD4^+$ T cells to HIV-2-infected MDMs resulted in lower levels of viral transfer to T cells compared to HIV-1-infected MDMs. The numerous viral particles present in the VCCs of HIV-2-infected MDMs suggested that neosynthesis of new viral progeny was not an issue. We titrated the particles produced by HIV-2-infected MDMs and found very low titres despite our use of a sensitive reporter cell line carrying a lacZ gene driven by the HIV-2-LTR. Infected MDMs appear to produce poorly infectious HIV-2 particles.

We next hypothesized that an inefficient counteraction of the restriction factor BST2 could explain both the defect in release of HIV-2 ROD9 and poor infectivity of the viral particles. The Env glycoprotein for HIV-2, and especially its cytoplasmic tail domain, is able to downregulate BST2 just as HIV-1 Vpu is (Kueck and Neil, 2012). The precise mechanisms involved in BST2 downregulation in HIV-2 infected macrophages remain elusive. To induce an HIV-1-like counteraction of BST2, MDMs were infected with either of the two HIV-2 strains alone or together with Vpu-Cherry. This led to a further reduction of BST2 total levels. However, Vpu-Cherry expression did not significantly improve the infectivity of the virions of both HIV-2 strains tested, suggesting little to no involvement of BST2 on the phenotypes observed. The moderate effects of Vpu on BST2 downregulation and on viral production in HIV-2-infected MDMs suggested that other unidentified restriction(s) or issue(s) impacted the HIV-2 cycle in MDMs. Finally, WT HIV-2 particles produced by HEK293FT cells (that do not express BST2), poorly infected primary $CD4^+$ T cells and indicated that the observed low rates of HIV-2 transfer from MDMs to $CD4^+$ T cells may have resulted in part from the poor natural infectivity of HIV-2 particles.

Macrophages possess the capacity to fuse and form syncytia under normal circumstances both *in vitro* and *in vivo* (Helming and Gordon, 2009; Helming et al., 2009). The resulting multigiant cells are endowed with capacities to engulf large complement-coated targets (Milde et al., 2015). HIV-1 infection through viral Env expression promotes cell-to-cell fusion resulting in syncytia formation (Clavel and Charneau, 1994; Kondo et al., 2015). We also frequently observed syncytia formation in our cultures of HIV-1 and -2-infected-MDMs. However, the contribution of macrophages syncytia to viral spreading remains to be evaluated *in vivo*. Transmission from infected T cells to macrophages has been reported to be an efficient way to promote the formation of multi-giant cells able to sustain important viral production *in vitro* (Bracq et al., 2017). It will be of interest to compare the capacity of HIV-1 and -2 in such an experimental setting.

Activated primary DCs resist HIV-1 infection but can capture and transfer the virus to $CD4^+$ T cells. In contrast, DCs are inefficient at transferring HIV-2 particles to $CD4^+$ T cells (Duvall et al., 2007; Kijewski et al., 2016). Therefore, both DC and macrophages appear to be inefficient at spreading HIV-2 infection to $CD4^+$ T cells. The mechanisms underlying the poor infectious capacity of the virions produced by HIV-2-infected macrophages appear complex and may involve sensing, unknown restriction- or macrophage-specific factors still yet to be identified.

The present *in vitro* study shows that HIV-2-infected MDMs can produce viral particles that accumulate in VCCs and are poorly infectious, raising the question of their role under

physiological conditions. If these features are conserved *in vivo*, tissue macrophages may contribute very poorly to the spread of HIV-2 infection. Future studies should determine whether infected macrophages can present HIV-2-derived antigens and stimulate specific T cells. The capacity of macrophages to directly present viral antigens on their MHC molecules could be affected by the viral protein Nef of HIV-2, although to different extend depending on the viral strain considered (Münch et al., 2005). As recently proposed, the restriction factor (TRIM5a), which efficiently promotes the degradation of HIV-2 Gag, may generate Gag epitopes suitable for efficient presentation by infected macrophages (Boswell and Rowland-Jones, 2019). Finally, macrophages could also sense incoming HIV-2 particles and provide inflammatory signals and viral antigens to dendritic cells which could in turn elicit strong cellular immune responses.

DATA AVAILABILITY STATEMENT

The raw data supporting the conclusions of this article will be made available by the authors, without undue reservation, to any qualified researcher.

ETHICS STATEMENT

Plasmapheresis residues were obtained from healthy adult donors (Etablissement Français du Sang, Paris, France), where all donors signed informed consent allowing the use of their blood for research purposes.

AUTHOR CONTRIBUTIONS

EG-M and PB designed the experiments and analysed the data. EG-M performed the experiments and built the Figures. NR set up the RT-qPCR for HIV genomic RNA quantification. LZ-T built the HIV-2*GagiGFP virus. MJ performed the EM analyses. MM performed the quantitative analysis of confocal microscopy images. VR provided elements to address concerns of the reviewers. EG-M, NR, and PB discussed the results and the plan of the manuscript. PB wrote the manuscript with the contribution of EG-M and NR. All authors read and approved the final manuscript.

FUNDING

This work was supported by grants from the "Agence Nationale de Recherche contre le SIDA et les hépatites virales" (ANRS), "Ensemble contre le SIDA" (Sidaction) 2018-1-AEQ-11984, ANR-10-IDEX-0001-02 PSL, and ANR-11-LABX-0043 to PB. EG-M was supported by ANRS doctoral fellowship and Foundation pour la Recherche Médicale (FRM) 4th year doctoral fellowship. NR was supported by post-doctoral fellowships from the ANRS and the FRM.

ACKNOWLEDGMENTS

We acknowledge the "plateforme d'imagerie cellulaire et tissulaire BioImaging de l'Institut Curie" (PICT-IBiSA) for access to the imaging facilities and the flow cytometry facility at Institut Curie. The authors thank Francesca Graziano, Xavier Lahaye, and Nicolas Manel at the Institut Curie, Bethany G. Charlton and Sarah Rowland-Jones at the University of Oxford for critical reading of the manuscript.

SUPPLEMENTARY MATERIAL

The Supplementary Material for this article can be found online at: https://www.frontiersin.org/articles/10.3389/fmicb.2020.01603/full#supplementary-material

REFERENCES

Achuthan, V., Singh, K., and DeStefano, J. J. (2017). Physiological Mg2+ conditions significantly alter the inhibition of HIV-1 and HIV-2 reverse transcriptases by nucleoside and non-nucleoside inhibitors in vitro. *Biochemistry* 56, 33–46. doi: 10.1021/acs.biochem.6b00943

Araínga, M., Edagwa, B., Mosley, R. L., Poluektova, L. Y., Gorantla, S., and Gendelman, H. E. (2017). A mature macrophage is a principal HIV-1 cellular reservoir in humanized mice after treatment with long acting antiretroviral therapy. *Retrovirology* 14:17. doi: 10.1186/s12977-017-0344-7

Bejarano, D. A., Puertas, M. C., Börner, K., Martinez-Picado, J., Müller, B., and Krausslich, H.-G. (2018). Detailed characterization of early HIV-1 replication dynamics in primary human macrophages. *Viruses* 10:620. doi: 10.3390/v10110620

Bennett, A. E., Narayan, K., Shi, D., Hartnell, L. M., Gousset, K., He, H., et al. (2009). Ion-abrasion scanning electron microscopy reveals surface-connected tubular conduits in HIV-infected macrophages. *PLoS Pathog.* 5:e1000591. doi: 10.1371/journal.ppat.1000591

Bèrre, S., Gaudin, R., Cunha, de Alencar, B., Desdouits, M., Chabaud, M., et al. (2013). CD36-specific antibodies block release of HIV-1 from infected primary macrophages and its transmission to T cells. *J. Exp. Med.* 210, 2523–2538. doi: 10.1084/jem.20130566

Boswell, M. T., and Rowland-Jones, S. L. (2019). Delayed disease progression in HIV-2: the importance of TRIM5α and the retroviral capsid. *Clin. Exp. Immunol.* 196, 305–317. doi: 10.1111/cei.13280

Bour, S., and Strebel, K. (2003). The HIV-1 Vpu protein: a multifunctional enhancer of viral particle release. *Microbes Infect.* 5, 1029–1039.

Bracq, L., Xie, M., Lambelé, M., Vu, L.-T., Matz, J., Schmitt, A., et al. (2017). T cell-macrophage fusion triggers multinucleated giant cell formation for HIV-1 spreading. *J. Virol.* 91:102. doi: 10.1128/JVI.01237-17

Chattergoon, M. A., Latanich, R., Quinn, J., Winter, M. E., Buckheit, R. W., Blankson, J. N., et al. (2014). HIV and HCV activate the inflammasome in monocytes and macrophages via endosomal Toll-like receptors without induction of type 1 interferon. *PLoS Pathog.* 10:e1004082. doi: 10.1371/journal.ppat.1004082

Chauveau, L., Donahue, D. A., Monel, B., Porrot, F., Bruel, T., Richard, L., et al. (2017). HIV fusion in dendritic cells occurs mainly at the surface and is limited by low CD4 levels. *J. Virol.* 91:344. doi: 10.1128/JVI.01248-17

Chertova, E., Chertov, O., Coren, L. V., Roser, J. D., Trubey, C. M., Bess, J. W., et al. (2006). Proteomic and biochemical analysis of purified human immunodeficiency virus type 1 produced from infected monocyte-derived macrophages. *J. Virol.* 80, 9039–9052. doi: 10.1128/JVI.01013-06

Clavel, F., and Charneau, P. (1994). Fusion from without directed by human immunodeficiency virus particles. *J. Virol.* 68, 1179–1185.

Clayton, K. L., Garcia, J. V., and Clements, J. E. (2017). HIV Infection of macrophages: implications for pathogenesis and cure. *Pathog. Immun.* 2:179. doi: 10.20411/pai.v2i2.204

Cribbs, S. K., Lennox, J., and Caliendo, A. M. (2015). Healthy HIV-1-infected individuals on highly active antiretroviral therapy harbor HIV-1 in their alveolar macrophages. *AIDS Res. Hum. Retroviruses* 31, 64–70. doi: 10.1089/aid.2014.0133

Cribier, A., Descours, B., Valadão, A., and Laguette, N. (2013). Phosphorylation of SAMHD1 by cyclin A2/CDK1 regulates its restriction activity toward HIV-1. *Cell Rep.* 3, 1036–1043. doi: 10.1016/j.celrep.2013.03.017

Damond, F., Gueudin, M., Pueyo, S., Farfara, I., Robertson, D. L., Descamps, D., et al. (2002). Plasma RNA viral load in human immunodeficiency virus type 2 subtype A and subtype B infections. *J. Clin. Microbiol.* 40, 3654–3659. doi: 10.1128/jcm.40.10.3654-3659.2002

De Clercq, E. (1993). HIV-1-specific RT inhibitors: highly selective inhibitors of human immunodeficiency virus type 1 that are specifically targeted at the viral reverse transcriptase. *Med. Res. Rev.* 13, 229–258. doi: 10.1002/med.26101 30303

de Silva, T. I., Aasa-Chapman, M., Cotten, M., Hué, S., Robinson, J., Bibollet-Ruche, F., et al. (2012). Potent autologous and heterologous neutralizing antibody responses occur in HIV-2 infection across a broad range of infection outcomes. *J. Virol.* 86, 930–946. doi: 10.1128/JVI.06126-11

de Silva, T. I., Peng, Y., Leligdowicz, A., Zaidi, I., Li, L., Griffin, H., et al. (2013). Correlates of T-cell-mediated viral control and phenotype of CD8(+) T cells in HIV-2, a naturally contained human retroviral infection. *Blood* 121, 4330–4339. doi: 10.1182/blood-2012-12-472787

Decalf, J., Desdouits, M., Rodrigues, V., Gobert, F.-X., Gentili, M., Marques-Ladeira, S., et al. (2017). Sensing of HIV-1 entry triggers a type I interferon response in human primary macrophages. *J. Virol.* 91:e147-17. doi: 10.1128/JVI.00147-17

Deneka, M., Pelchen-Matthews, A., Byland, R., Ruiz-Mateos, E., and Marsh, M. (2007). In macrophages, HIV-1 assembles into an intracellular plasma membrane domain containing the tetraspanins CD81, CD9, and CD53. *J. Cell Biol.* 177, 329–341. doi: 10.1083/jcb.200609050

Descours, B., Cribier, A., Chable-Bessia, C., Ayinde, D., Rice, G., Crow, Y., et al. (2012). SAMHD1 restricts HIV-1 reverse transcription in quiescent CD4(+) T-cells. *Retrovirology* 9:87. doi: 10.1186/1742-4690-9-87

Duvall, M. G., Loré, K., Blaak, H., Ambrozak, D. A., Adams, W. C., Santos, K., et al. (2007). Dendritic cells are less susceptible to human immunodeficiency virus type 2 (HIV-2) infection than to HIV-1 infection. *J. Virol.* 81, 13486–13498. doi: 10.1128/JVI.00976-07

Esbjörnsson, J., Jansson, M., Jespersen, S., Månsson, F., Hønge, B. L., Lindman, J., et al. (2019). HIV-2 as a model to identify a functional HIV cure. *AIDS Res. Ther.* 16:24. doi: 10.1186/s12981-019-0239-x

Fernandes, S. M., Pires, A. R., Ferreira, C., Tendeiro, R., Correia, L., Paulo, S. E., et al. (2014). Gut disruption in HIV-2 infection despite reduced viremia. *AIDS* 28, 290–292. doi: 10.1097/QAD.0000000000000114

Freed, E. O., and Martin, M. A. (1995). The role of human immunodeficiency virus type 1 envelope glycoproteins in virus infection. *JBC* 270, 23883–23886. doi: 10.1074/jbc.270.41.23883

Ganor, Y., Real, F., Sennepin, A., Dutertre, C.-A., Prevedel, L., Xu, L., et al. (2019). HIV-1 reservoirs in urethral macrophages of patients under suppressive antiretroviral therapy. *Nat. Microbiol* 48:872. doi: 10.1038/s41564-018-0335-z

Gao, F., Yue, L., Robertson, D. L., Hill, S. C., Hui, H., Biggar, R. J., et al. (1994). Genetic diversity of human immunodeficiency virus type 2: evidence for distinct sequence subtypes with differences in virus biology. *J. Virol.* 68, 7433–7447.

Gaudin, R., Berre, S., Cunha, de Alencar, B., Decalf, J., Schindler, M., et al. (2013). Dynamics of HIV-containing compartments in macrophages reveal sequestration of virions and transient surface connections. *PLoS ONE* 8:e69450. doi: 10.1371/journal.pone.0069450

Gousset, K., Ablan, S. D., Coren, L. V., Ono, A., Soheilian, F., Nagashima, K., et al. (2008). Real-time visualization of HIV-1 GAG trafficking in infected macrophages. *PLoS Pathog.* 4:e1000015. doi: 10.1371/journal.ppat.1000015

Graziano, F., Desdouits, M., Garzetti, L., Podini, P., Alfano, M., Rubartelli, A., et al. (2015). Extracellular ATP induces the rapid release of HIV-1 from virus containing compartments of human macrophages. *Proc. Natl. Acad. Sci. U.S.A.* 112, E3265–E3273. doi: 10.1073/pnas.1500656112

Hauser, H., Lopez, L. A., Yang, S. J., Oldenburg, J. E., Exline, C. M., Guatelli, J. C., et al. (2010). HIV-1 Vpu and HIV-2 Env counteract BST-2/tetherin by sequestration in a perinuclear compartment. *Retrovirology* 7:51. doi: 10.1186/1742-4690-7-51

Helming, L., and Gordon, S. (2009). Molecular mediators of macrophage fusion. *Trends Cell Biol.* 19, 514–522. doi: 10.1016/j.tcb.2009.07.005

Helming, L., Winter, J., and Gordon, S. (2009). The scavenger receptor CD36 plays a role in cytokine-induced macrophage fusion. *J. Cell Sci.* 122, 453–459. doi: 10.1242/jcs.037200

Hollenbaugh, J. A., Montero, C., Schinazi, R. F., Munger, J., and Kim, B. (2016). Metabolic profiling during HIV-1 and HIV-2 infection of primary human monocyte-derived macrophages. *Virology* 491, 106–114. doi: 10.1016/j.virol.2016.01.023

Honeycutt, J. B., Thayer, W. O., Baker, C. E., Ribeiro, R. M., Lada, S. M., Cao, Y., et al. (2017). HIV persistence in tissue macrophages of humanized myeloid-only mice during antiretroviral therapy. *Nat Med.* 23, 638–643. doi: 10.1038/nm.4319

Honeycutt, J. B., Wahl, A., Baker, C., Spagnuolo, R. A., Foster, J., Zakharova, O., et al. (2016). Macrophages sustain HIV replication in vivo independently of T cells *J. Clin. Invest.* 126, 1353–1366. doi: 10.1172/JCI84456

Houzet, L., Morichaud, Z., and Mougel, M. (2007). Fully-spliced HIV-1 RNAs are reverse transcribed with similar efficiencies as the genomic RNA in virions and cells, but more efficiently in AZT-treated cells. *Retrovirology* 4:30. doi: 10.1186/1742-4690-4-30

Hrecka, K., Hao, C., Gierszewska, M., Swanson, S. K., Kesik-Brodacka, M., Srivastava, S., et al. (2011). Vpx relieves inhibition of HIV-1 infection of macrophages mediated by the SAMHD1 protein. *Nature* 474, 658–661. doi: 10.1038/nature10195

Hubner, W., Chen, P., Del Portillo, A., Liu, Y., Gordon, R. E., and Chen, B. K. (2007). Sequence of human immunodeficiency virus type 1 (HIV-1) Gag localization and oligomerization monitored with live confocal imaging of a replication-competent, fluorescently tagged HIV-1. *J. Virol.* 81, 12596–12607. doi: 10.1128/JVI.01088-07

Igarashi, T., Brown, C. R., Endo, Y., Buckler-White, A., Plishka, R., Bischofberger, N., et al. (2001). Macrophage are the principal reservoir and sustain high virus loads in rhesus macaques after the depletion of CD4+ T cells by a highly pathogenic simian immunodeficiency virus/HIV type 1 chimera (SHIV): implications for HIV-1 infections of humans. *Proc. Natl. Acad. Sci. U.S.A.* 98, 658–663. doi: 10.1073/pnas.021551798

James, K. L., de Silva, T. I., Brown, K., Whittle, H., Taylor, S., McVean, G., et al. (2019). Low-Bias RNA sequencing of the HIV-2 genome from blood plasma. *J. Virol.* 93:588. doi: 10.1128/JVI.00677-18

Jouve, M., Sol-Foulon, N., Watson, S., Schwartz, O., and Benaroch, P. (2007). HIV-1 buds and accumulates in "nonacidic" endosomes of macrophages. 2, 85–95. doi: 10.1016/j.chom.2007.06.011

Kandathil, A. J., Sugawara, S., Goyal, A., Durand, C. M., Quinn, J., Sachithanandham, J., et al. (2018). No recovery of replication-competent HIV-1 from human liver macrophages. *J. Clin. Invest.* 128, 4501–4509. doi: 10.1172/JCI121678

Kijewski, S. D. G., Akiyama, H., Feizpour, A., Miller, C. M., Ramirez, N.-G. P., Reinhard, B. M., et al. (2016). Access of HIV-2 to CD169-dependent dendritic cell-mediated trans infection pathway is attenuated. *Virology* 497, 328–336. doi: 10.1016/j.virol.2016.07.029

Kondo, N., Marin, M., Kim, J. H., Desai, T. M., and Melikyan, G. B. (2015). Distinct requirements for HIV-cell fusion and HIV-mediated cell-cell fusion. *J. Biol. Chem.* 290, 6558–6573. doi: 10.1074/jbc.M114.623181

Koppensteiner, H., Brack-Werner, R., and Schindler, M. (2012). Macrophages and their relevance in human immunodeficiency virus type I infection. *Retrovirology* 9:82. doi: 10.1186/1742-4690-9-82

Kruize, Z., and Kootstra, N. A. (2019). The role of macrophages in HIV-1 persistence and pathogenesis. *Front. Microbiol.* 10:2828. doi: 10.3389/fmicb.2019.02828

Kueck, T., and Neil, S. J. D. (2012). A cytoplasmic tail determinant in HIV-1 Vpu mediates targeting of tetherin for endosomal degradation and counteracts interferon-induced restriction. *PLoS Pathog.* 8:e1002609. doi: 10.1371/journal.ppat.1002609

Laguette, N., Sobhian, B., Casartelli, N., and Ringeard, M. (2011). SAMHD1 is the dendritic–and myeloid–cell–specific HIV–1 restriction factor counteracted by Vpx. *Nature* 474, 654–657. doi: 10.1038/nature10117

Lahaye, X., Satoh, T., Gentili, M., Cerboni, S., Conrad, C., Hurbain, I., et al. (2013). The capsids of HIV-1 and HIV-2 determine immune detection of the viral cDNA by the innate sensor cGAS in dendritic cells. *Immunity* 39, 1132–1142. doi: 10.1016/j.immuni.2013.11.002

Le Tortorec, A., and Neil, S. J. D. (2009). Antagonism to and intracellular sequestration of human tetherin by the human immunodeficiency virus type 2 envelope glycoprotein. *J. Virol.* 83, 11966–11978. doi: 10.1128/JVI.01515-09

Leligdowicz, A., Yindom, L.-M., Onyango, C., Sarge-Njie, R., Alabi, A., Cotten, M., et al. (2007). Robust gag-specific T cell responses characterize viremia control in HIV-2 infection. *J. Clin. Invest.* 117, 3067–3074. doi: 10.1172/JCI32380

Manel, N., Hogstad, B., Wang, Y., Levy, D. E., Unutmaz, D., and Littman, D. R. (2010). A cryptic sensor for HIV-1 activates antiviral innate immunity in dendritic cells. *Nature* 467, 214–217. doi: 10.1038/nature09337

Marchant, D., Neil, S. J. D., and McKnight, A. (2006). Human immunodeficiency virus types 1 and 2 have different replication kinetics in human primary macrophage culture. *J. Gen. Virol.* 87, 411–418. doi: 10.1099/vir.0.81391-0

Marlink, R., Kanki, P., Thior, I., Travers, K., Eisen, G., Siby, T., et al. (1994). Reduced rate of disease development after HIV-2 infection as compared to HIV-1. *Science* 265, 1587–1590. doi: 10.1126/science.7915856

Mazzolini, J., Herit, F., Bouchet, J., Benmerah, A., Benichou, S., and Niedergang, F. (2010). Inhibition of phagocytosis in HIV-1-infected macrophages relies on Nef-dependent alteration of focal delivery of recycling compartments. *Blood* 115, 4226–4236. doi: 10.1182/blood-2009-12-259473

Milde, R., Ritter, J., Tennent, G. A., Loesch, A., Martinez, F. O., Gordon, S., et al. (2015). Multinucleated giant cells are specialized for complement-mediated phagocytosis and large target destruction. *CellReports* 13, 1937–1948. doi: 10.1016/j.celrep.2015.10.065

Münch, J., Schindler, M., Wildum, S., Rücker, E., Bailer, N., Knoop, V., et al. (2005). Primary sooty mangabey simian immunodeficiency virus and human immunodeficiency virus type 2 nef alleles modulate cell surface expression of various human receptors and enhance viral infectivity and replication. *J. Virol.* 79, 10547–10560. doi: 10.1128/JVI.79.16.10547-10560.2005

Nasr, N., Alshehri, A. A., Wright, T. K., Shahid, M., Heiner, B. M., Harman, A. N., et al. (2017). Mechanism of interferon stimulated gene induction in HIV-1 infected macrophages. *J. Virol.* 91:e00744-17. doi: 10.1128/JVI.00744-17

Neil, S., Zang, T., and Nature, P. B. (2008). Tetherin inhibits retrovirus release and is antagonized by HIV-1 Vpu. *Nature* 451, 425–430. doi: 10.1038/nature06553

Neil, S. J. D., Sandrin, V., Sundquist, W. I., and Bieniasz, P. D. (2007). An interferon-alpha-induced tethering mechanism inhibits HIV-1 and Ebola virus particle release but is counteracted by the HIV-1 Vpu protein. 2, 193–203. doi: 10.1016/j.chom.2007.08.001

Nyamweya, S., Hegedus, A., Jaye, A., Rowland-Jones, S., Flanagan, K. L., and Macallan, D. C. (2013). Comparing HIV-1 and HIV-2 infection: lessons for viral immunopathogenesis. *Rev. Med. Virol.* 23, 221–240. doi: 10.1002/rmv.1739

Ono, A. (2010). HIV-1 assembly at the plasma membrane. *Vaccine* 28(Suppl. 2), B55–B59. doi: 10.1016/j.vaccine.2009.10.021

Ono, A., Ablan, S. D., Lockett, S. J., Nagashima, K., and Freed, E. O. (2004). Phosphatidylinositol (4,5) bisphosphate regulates HIV-1 Gag targeting to the plasma membrane. *Proc. Natl. Acad. Sci. U.S.A.* 101, 14889–14894. doi: 10.1073/pnas.0405596101

Pelchen-Matthews, A., Giese, S., Mlčochová, P., Turner, J., and Marsh, M. (2012). β2 integrin adhesion complexes maintain the integrity of HIV-1 assembly compartments in primary macrophages. *Traffic* 13, 273–291. doi: 10.1111/j.1600-0854.2011.01306.x

Pelchen-Matthews, A., Kramer, B., and Marsh, M. (2003). Infectious HIV-1 assembles in late endosomes in primary macrophages. *J. Cell Biol.* 162, 443–455. doi: 10.1083/jcb.200304008

Popper, S. J., Sarr, A. D., Guèye-Ndiaye, A., Mboup, S., Essex, M. E., and Kanki, P. J. (2000). Low plasma human immunodeficiency virus type 2 viral load is independent of proviral load: low virus production in vivo. *J. Virol.* 74, 1554–1557. doi: 10.1128/jvi.74.3.1554-1557.2000

Rodrigues, V., Ruffin, N., San-Roman, M., and Benaroch, P. (2017). Myeloid cell interaction with HIV: a complex relationship. *Front. Immunol.* 8:1698. doi: 10.3389/fimmu.2017.01698

Rowland-Jones, S. L., and Whittle, H. C. (2007). Out of Africa: what can we learn from HIV-2 about protective immunity to HIV-1? *Nat. Immunol.* 8, 329–331. doi: 10.1038/ni0407-329

Schindelin, J., Arganda-Carreras, I., Frise, E., Kaynig, V., Longair, M., Pietzsch, T., et al. (2012). Fiji: an open-source platform for biological-image analysis. *Nat. Methods* 9, 676–682. doi: 10.1038/nmeth.2019

Silvin, A., Yu, C. I., Lahaye, X., Imperatore, F., Brault, J.-B., Cardinaud, S., et al. (2017). Constitutive resistance to viral infection in human CD141+ dendritic cells. *Sci. Immunol.* 2:eaai8071. doi: 10.1126/sciimmunol.aai8071

Soares, R. S., Tendeiro, R., Foxall, R. B., Baptista, A. P., Cavaleiro, R., Gomes, P., et al. (2011). Cell-associated viral burden provides evidence of ongoing viral replication in aviremic HIV-2-infected patients. *J. Virol.* 85, 2429–2438. doi: 10.1128/JVI.01921-10

Sunseri, N., O'Brien, M., Bhardwaj, N., and Landau, N. R. (2011). Human immunodeficiency virus type 1 modified to package Simian immunodeficiency virus Vpx efficiently infects macrophages and dendritic cells. *J. Virol.* 85, 6263–6274. doi: 10.1128/JVI.00346-11

Swingler, S., Mann, A. M., Zhou, J., Swingler, C., and Stevenson, M. (2007). Apoptotic killing of HIV-1-infected macrophages is subverted by the viral envelope glycoprotein. *PLoS Pathog.* 3:e134. doi: 10.1371/journal.ppat.0030134

van der Loeff, M. F. S., Larke, N., Kaye, S., Berry, N., Ariyoshi, K., Alabi, A., et al. (2010). Undetectable plasma viral load predicts normal survival in HIV-2-infected people in a West African village. *Retrovirology* 7:46. doi: 10.1186/1742-4690-7-46

Verollet, C., Souriant, S., Bonnaud, E., Jolicoeur, P., Raynaud-Messina, B., Kinnaer, C., et al. (2014). HIV-1 reprograms the migration of macrophages. *Blood* 125, 1611–1622. doi: 10.1182/blood-2014-08-596775

Wacleche, V. S., Tremblay, C. L., Routy, J.-P., and Ancuta, P. (2018). The biology of monocytes and dendritic cells: contribution to HIV pathogenesis. *Viruses* 10:65. doi: 10.3390/v10020065

Conflict of Interest: The authors declare that the research was conducted in the absence of any commercial or financial relationships that could be construed as a potential conflict of interest.